Synaptotagmin oligomerization is essential for calcium control of regulated exocytosis

Oscar D. Bello[a,b,1], Ouardane Jouannot[a,1], Arunima Chaudhuri[a], Ekaterina Stroeva[a], Jeff Coleman[a], Kirill E. Volynski[b], James E. Rothman[a,b,2], and Shyam S. Krishnakumar[a,b,2]

[a]Department of Cell Biology, Yale University School of Medicine, New Haven, CT 06520; and [b]Department of Clinical and Experimental Epilepsy, Institute of Neurology, University College London, WC1N 3BG London, United Kingdom

Contributed by James E. Rothman, June 22, 2018 (sent for review May 22, 2018; reviewed by Vivek Malhotra and Thomas Söllner)

Regulated exocytosis, which underlies many intercellular signaling events, is a tightly controlled process often triggered by calcium ion(s) (Ca^{2+}). Despite considerable insight into the central components involved, namely, the core fusion machinery [soluble *N*-ethylmaleimide–sensitive factor attachment protein receptor (SNARE)] and the principal Ca^{2+} sensor [C2-domain proteins like synaptotagmin (Syt)], the molecular mechanism of Ca^{2+}-dependent release has been unclear. Here, we report that the Ca^{2+}-sensitive oligomers of Syt1, a conserved structural feature among several C2-domain proteins, play a critical role in orchestrating Ca^{2+}-coupled vesicular release. This follows from pHluorin-based imaging of single-vesicle exocytosis in pheochromocytoma (PC12) cells showing that selective disruption of Syt1 oligomerization using a structure-directed mutation (F349A) dramatically increases the normally low levels of constitutive exocytosis to effectively occlude Ca^{2+}-stimulated release. We propose a parsimonious model whereby Ca^{2+}-sensitive oligomers of Syt (or a similar C2-domain protein) assembled at the site of docking physically block spontaneous fusion until disrupted by Ca^{2+}. Our data further suggest Ca^{2+}-coupled vesicular release is triggered by removal of the inhibition, rather than by direct activation of the fusion machinery.

regulated exocytosis | synaptotagmin | SNARE protein | calcium | PC12 cells

Timely secretion of a variety of critical molecules, including neurotransmitters, hormones, and enzymes, is achieved via regulated exocytosis (1–3). During regulated exocytosis, the secretory vesicles fuse to the plasma membrane (PM) in response to external stimuli, typically activated by calcium ion (Ca^{2+}) influx. However, soluble *N*-ethylmaleimide–sensitive factor attachment protein receptor (SNARE) proteins, which catalyze the fusion of the cargo-carrying vesicles, are constitutively active (4, 5). When the cognate pair of SNAREs located on the vesicle and the target membrane are in molecular proximity, they readily assemble into a stable complex providing the energy to fuse the membranes (4, 5). Thus, regulated exocytosis requires mechanisms both to prevent the spontaneous fusion of vesicles ("clamping") under rest and to transduce the Ca^{2+} signal into activating the clamped fusion machinery (1–3).

Synaptotagmins (Syt), a family of tandem C2-domain (C2A and C2B)–containing protein that binds both Ca^{2+} and SNARE proteins (3, 6–10), play a critical role in this process. The Ca^{2+} activation mechanism has been well characterized and involves the insertion of surface loops on each of the C2 domains into the membrane bilayer, with Ca^{2+} coordinating it to acidic lipids, phosphatidylserine (PS), and phosphatidylinositol 4,5-bisphosphate (PIP2) (11–16). However, how the constitutive fusion is arrested to enable Ca^{2+}-coupled exocytosis is not known. Nevertheless, Syt is believed to play a crucial role in this process, as deletion (or mutations) of Syt1 (the neuronal isoform), in addition to eliminating the Ca^{2+}-dependent release, increases the normally small rate of spontaneous exocytosis (8, 17).

New details on the spatial organization of Syt1 (and related C2-domain proteins) have recently emerged, which could potentially describe its dual role in orchestrating regulated exocytosis (18–21). Isolated Syt1 was discovered to polymerize into ∼30-nm (diameter)-sized ring-like oligomers, prompted by the binding of polyvalent anions, such as ATP in solution or PS/PIP2 on membranes, to a conserved polylysine motif within the C2B domain (19–21). Moreover, the ring-shaped oligomers formed on membranes are sensitive to Ca^{2+} and rapidly disassemble at a physiological Ca^{2+} concentration. This is because the same surface on the C2B domain that is used to form the ring binds Ca^{2+} and reorients into the lipid bilayer (19, 21). If these C2B-derived Syt1 oligomers were to form at the site of docking, then they could potentially regulate the terminal phases of vesicular release (18). While there is yet no direct evidence that such ring oligomers exist in vivo, salient genetic and biochemical correlates provided by the oligomeric structure (19, 21) and the structural conservation of circular oligomerization among many C2-domain proteins (21) strongly support the overall hypothesis.

In this report, we examine the physiological role of the Syt1 oligomers using a targeted mutation (F349A) that specifically disrupts the C2B-dependent oligomerization. We find that destabilizing the Syt1 oligomers uncouples vesicular release from Ca^{2+} influx in pheochromocytoma (PC12) cells, even though the Ca^{2+}-sensing capacity and other molecular properties of Syt1 are unaltered. Our data suggest that the Syt1 oligomerization represents a central organizing principle for Ca^{2+}-coupled exocytosis in PC12 cells and may very well represent a universal mechanism underlying Ca^{2+}-regulated exocytosis under diverse settings.

Significance

Synaptotagmin (Syt) is the primary calcium ion (Ca^{2+}) sensor for regulated exocytosis. It couples Ca^{2+} binding to soluble *N*-ethylmaleimide–sensitive factor attachment protein receptor-catalyzed fusion, but how this happens is unclear. Here, using a targeted mutation combined with a single-vesicle fusion optical assay, we show that the recently discovered structural feature of Syt to self-oligomerize is essential for Ca^{2+} coupling of vesicular fusion. This suggests an elegant yet simple model in which these Syt oligomers formed at the interface of the docked vesicle physically prevent fusion until the influx of Ca^{2+}.

Author contributions: O.D.B., O.J., A.C., E.S., J.E.R., and S.S.K. designed research; O.D.B., O.J., A.C., and E.S. performed research; J.C. contributed new reagents/analytic tools; O.D.B., O.J., A.C., E.S., K.E.V., J.E.R., and S.S.K. analyzed data; and O.D.B., O.J., A.C., K.E.V., J.E.R., and S.S.K. wrote the paper.

Reviewers: V.M., The Barcelona Institute of Science and Technology; and T.S., University of Heidelberg.

The authors declare no conflict of interest.

[1]O.D.B. and O.J. contributed equally to this work.

[2]To whom correspondence may be addressed. Email: james.rothman@yale.edu or shyam.krishnakumar@yale.edu.

This article contains supporting information online at www.pnas.org/lookup/suppl/doi:10.1073/pnas.1808792115/-/DCSupplemental.

Published online July 23, 2018.

Results

Identification of Syt1 Ring Oligomer-Disrupting Mutation. To test the functional role of the Syt1 oligomers, we sought to generate targeted mutations in Syt1 that specifically disrupt its C2B-dependent oligomerization. Based on fitting the X-ray crystal structure of Syt1^{C2AB} (residues 143–421) into the electron microscopy (EM) density map generated from the reconstruction of the Syt1^{C2AB}-coated tubes (19) (*SI Appendix*, Fig. S1*A*), we identified putative residues in the C2B domain (Val-304, Leu-307, Tyr-311, Phe-349, and Leu-394) likely to be involved in mediating Syt1 ring oligomer assembly (Fig. 1*A*). Given the hydrophobic nature of the dimer interface (Fig. 1*A*), we systematically assessed the effect of polar (Asn) mutation on oligomer assembly using EM analysis as described previously (19, 21).

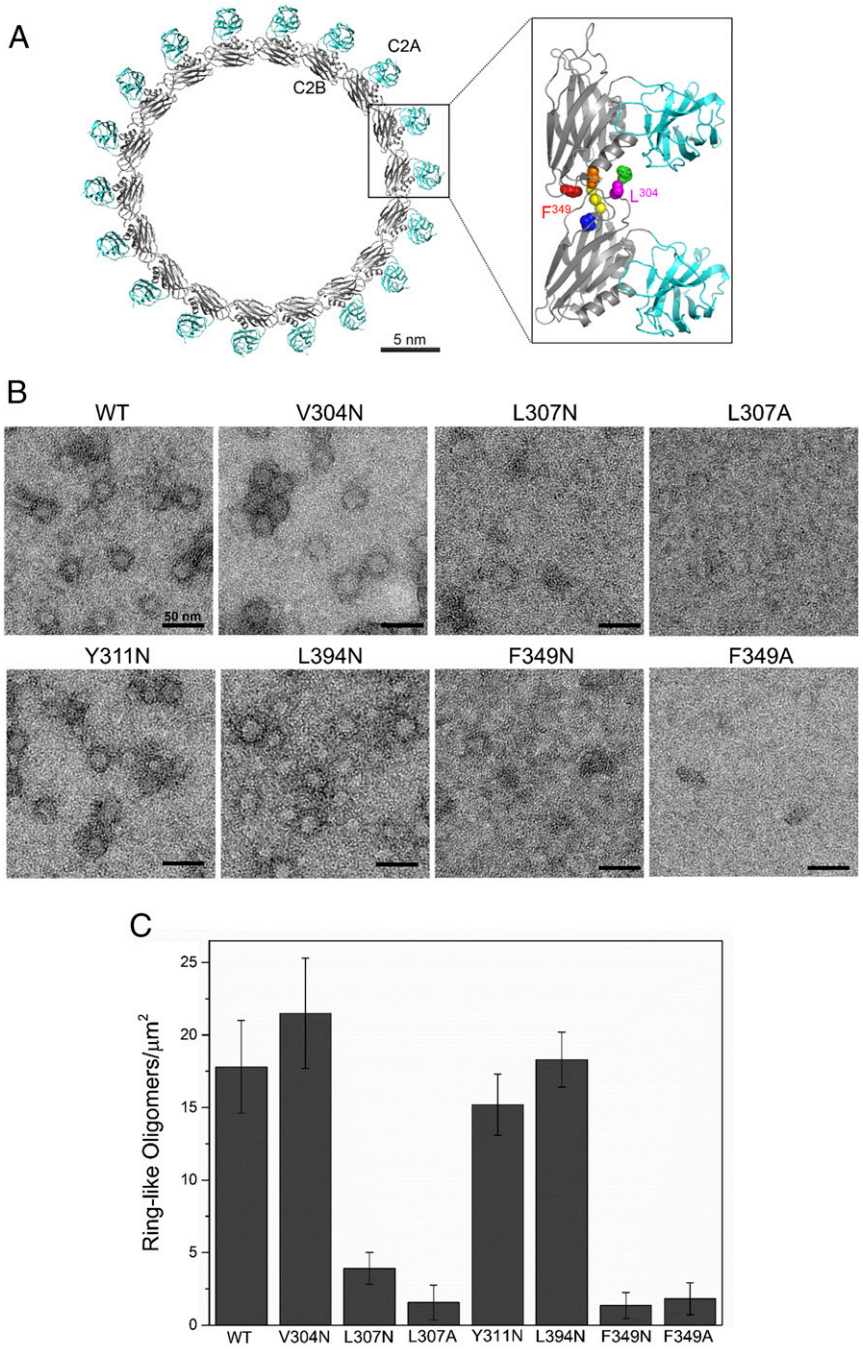

Fig. 1. Identification of the Syt1 ring oligomer-disrupting mutation. (*A*) Reconstruction of the Syt1 ring-like oligomer (19) shows that the interaction of the C2B domain (gray) drives oligomerization, with the Ca^{2+} loops (yellow) locating to the dimer interface, while the C2A domain (cyan) appends the C2B ring oligomer. (*B* and *C*) Mutational analysis of the key hydrophobic residues locating to the oligomeric interface showing alteration of Leu-307 (*A*, *Inset*; magenta) and Phe-349 (*A*, *Inset*; red) residues significantly reduces the number of oligomers formed with the minimal C2AB domain (Syt1^{C2AB}) on the lipid monolayer (60:40 PC/PS) as visualized by negative-stain EM analysis. Mutation of other putative residues, Val-304 (*A*, *Inset*; green), Tyr-311 (*A*, *Inset*; blue), or Leu-394 (*A*, *Inset*; orange), showed no effect on the Syt1^{C2AB} polymerization. Representative micrographs are shown, and average and deviations from three independent experiments are included.

Briefly, the lipid monolayer (PC/PS at a 3:2 molar ratio) formed at the air/water interface was recovered on a carbon-coated EM grid, and protein solution was added to the lipid monolayer under Ca^{2+}-free conditions (1 mM EDTA) and incubated for 1 min at 37 °C. Negative-stain analysis revealed that polar (Asn) mutation of two key hydrophobic residues (Leu-307 and Phe-349) has a strong effect, with a near-complete elimination of $Syt1^{C2AB}$ oligomeric structures (Fig. 1 *B* and *C*). Similar mutation of other putative residues had little or no effect on the $Syt1^{C2AB}$ polymerization (Fig. 1 *B* and *C*). In fact, replacing Leu-307 or Phe-349 with a weak hydrophobic residue, such as Ala (L307A or F349A), was sufficient to disrupt the oligomer formation (Fig. 1 *B* and *C*). Given the conservative nature of the Ala replacement and lower probability of off-target effects, we chose these mutations for further analysis.

F349A Mutation Selectively Affects Syt1 Oligomerization. To evaluate the specificity of the identified mutations, we examined the effect of L307A ($Syt1^{L307A}$) and F349A ($Syt1^{F349A}$) mutation on distinct molecular properties of Syt1 (Fig. 2). Microscale thermophoresis (MST) analysis (Fig. 2*A*) using Alexa Fluor 488-labeled Syt1 (residue 269) revealed a comparable intrinsic Ca^{2+} affinity for $Syt1^{WT}$ [Ca^{2+}-binding constant (K_{Ca}) = 235.3 ± 85.6 μM] and $Syt1^{F349A}$ (K_{Ca} = 226.8 ± 40.4 μM), but a weaker binding for $Syt1^{L307A}$ mutant (K_{Ca} = 922.5 ± 83.3 μM). Since Leu-307 residue locates within the Ca^{2+}-binding loops on the Syt1 C2B domain, a mutation at this site might affect the Ca^{2+} coordination properties of the C2B domain. Thus, we chose to focus on the F349A mutation, which does not locate within any known functional surface of Syt1, for further analysis.

A lipid-binding assay showed that $Syt1^{F349A}$ readily binds PS/PIP2-containing liposomes under Ca^{2+}-free conditions and to levels comparable to the WT ($Syt1^{WT}$) (Fig. 2*B*). This indicates that the electrostatic interaction between the conserved polylysine motifs on C2B and the anionic lipids, which is needed for the close docking of vesicles to the PM under both in vitro and in vivo conditions (14, 22–24), is unaltered by the F349A mutation. Stopped-flow rapid mixing analysis (Fig. 2*C*) using the environment-sensitive fluorescent probe 7-nitrobenz-2-oxa-1,3-diazol-4-yl-ethylenediamine (NBD)

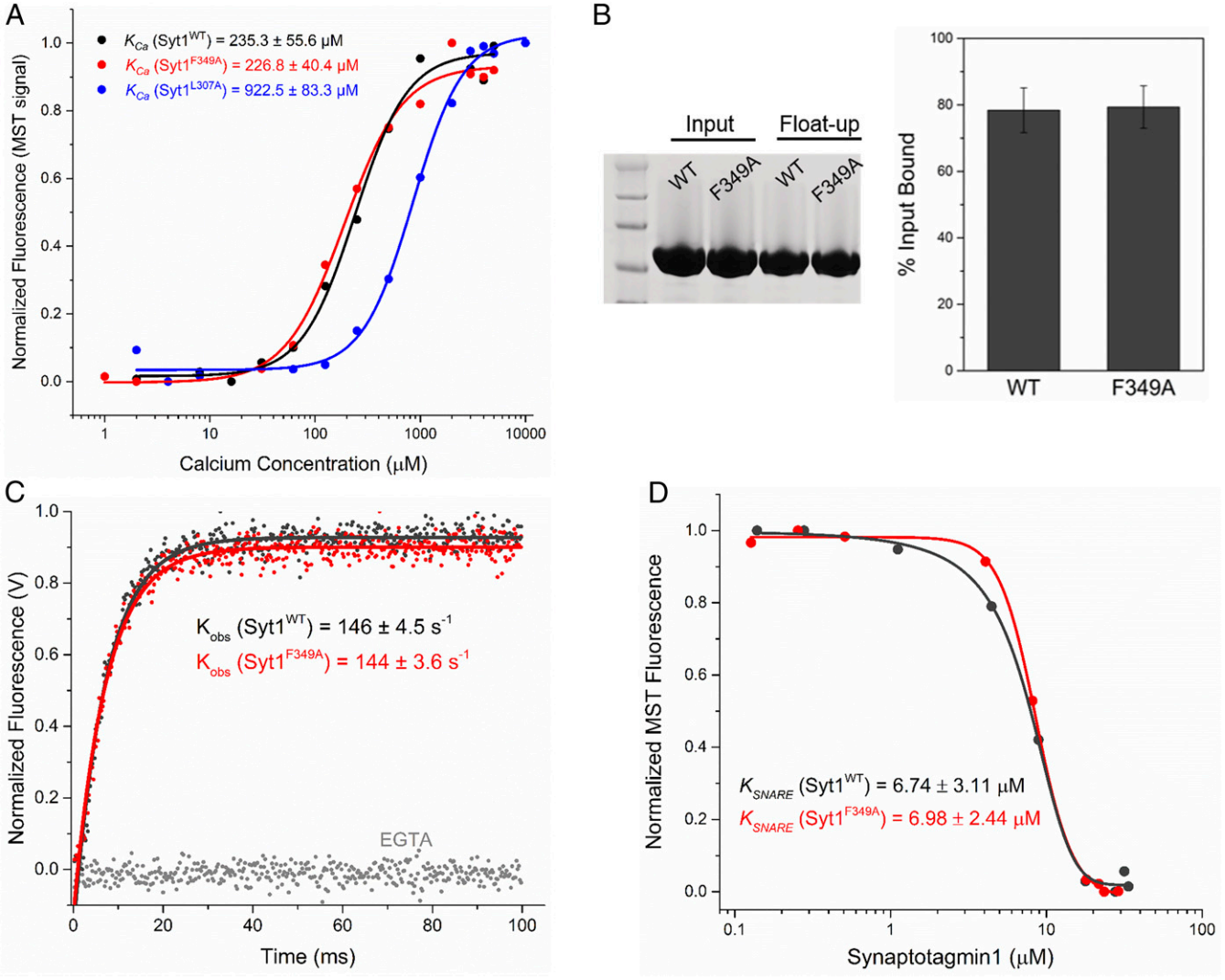

Fig. 2. F349A mutation selectively disrupts Syt1 oligomerization. (*A*) Ca^{2+} binding measured by MST analysis using Alexa Fluor 488-labeled (residue 269) Syt1 shows that the L307A mutation (blue) lowers the intrinsic Ca^{2+} affinity but the F349A mutation (red) has no effect compared with WT (black). The F349A mutation also does not affect other molecular properties, namely, Ca^{2+}-independent lipid binding examined by liposome flotation analysis (*B*), Ca^{2+}-triggered membrane interaction of the C2B domain tracked by stopped-flow rapid mixing analysis with the environment-sensitive fluorescent probe NBD attached to the C2B-domain residue V304C (*C*), and the ability to bind the SNARE complex assessed by MST analysis using Alexa Fluor 488-labeled SNARE complex (*D*; VAMP2 residue 28). A representative gel and curves are shown, and the average and deviation from three independent experiments are included.

attached to the membrane-penetrating loop of the C2B domain (residue V304C) showed that both the Syt1^{WT} and Syt1^{F349A} insert very rapidly into the bilayer upon Ca^{2+} binding, and with similar kinetics [observed rate of loop insertion (k_{obs}) = 146 ± 4.5 s^{-1} and k_{obs} = 144 ± 3.6 s^{-1}, respectively]. Likewise, MST analysis using Alexa Fluor 488-labeled SNARE complex (VAMP2 residue 28) exhibited comparable binding affinity [SNARE-binding constant (K_{SNARE}) ~ 7 μM] to both Syt1^{WT} and Syt1^{F349A}, implying that Syt1–SNARE interaction is unchanged (Fig. 2*D*). This implies that F349A mutation selectively impairs Syt1 oligomerization without affecting other critical molecular properties. Further underscoring its effectiveness, the F349A mutation also disrupted the ring oligomer formation of the entire cytoplasmic domain of Syt1 (residues 96–421) under physiological lipid and buffer conditions (*SI Appendix*, Fig. S1*B*).

F349A Mutation Eliminates Ca^{2+} Control of Exocytosis in PC12 Cells. We assessed the effect of the F349A mutation on vesicular exocytosis using rat adrenal PC12 cells, a widely used model system for studying neurosecretion (25, 26). Specifically, we expressed both Syt1^{WT} and Syt1^{F349A} in a Syt1-deficient PC12 cell line (F7 cells) (27) and performed live-cell total internal reflection fluorescence microscopy (TIRFM) imaging to monitor single exocytotic events by employing pHluorin-tagged (luminal) VAMP2 (28–31) (Fig. 3). We chose VAMP2-pHluorin as a fusion reporter because it serves as a universal marker for all vesicle types (small clear vesicles and small and large dense-core vesicles) in PC12 cells, and in our TIRFM setup, the pHluorin signal increase corresponding to a fusion event can be automatically detected and scored by differential analysis of the images (29–31).

Quantitative immunoblot analysis (Fig. 3*A* and *SI Appendix*, Fig. S2) and immunofluorescence analysis (Fig. 3*B*) of the untransfected F7 cells (with normal PC12 cells as a reference) confirmed the absence of Syt1 expression, but also revealed a significant reduction (~50%) in the expression of Syt9, a closely related isoform implicated in mediating Ca^{2+}-dependent release in PC12 cells (32). Correspondingly, untransfected F7 cells showed a significant reduction in the number of fusion events compared with the control PC12 cells. Notably, both the constitutive and Ca^{2+}-stimulated vesicle fusion was diminished (Fig. 3*C*), hinting at possible impairment of the vesicle docking/priming process. This was confirmed by EM data showing a significant reduction of vesicle density in the immediate vicinity of the PM in the F7 cells (Fig. 3*D*).

Overexpression of Syt1^{WT} in this background partially rescued vesicle docking (Fig. 3*D*) and restored the fusion properties to the control levels (Fig. 3*C*). In particular, it reestablished the Ca^{2+} control of exocytosis with a low rate of constitutive exocytotic events (approximately three events per minute) compared with robust regulated exocytosis (~10 fusion events per minute) when triggered by KCl depolarization in the presence of Ca^{2+}. This strictly required Ca^{2+} binding to Syt1, specifically to the C2B domain, as disrupting its Ca^{2+}-binding ability using targeted mutations (D309A, D363A, D365A; Syt1^{3A}) completely abolished the Ca^{2+}-induced enhancement of vesicular release (Fig. 3*C*).

Syt1^{F349A} similarly rescued the docking phenotype, with the density and distribution of vesicles very similar to the Syt1^{WT} (Fig. 3*D*). However, the number of spontaneous exocytotic events under resting conditions increased approximately threefold compared to rescue with the Syt1^{WT} construct (Fig. 3*C*). Strikingly, Syt1^{F349A} overexpression occluded the Ca^{2+}-dependent increase of vesicular exocytosis triggered by KCl depolarization (Fig. 3*C*). In essence, the F349A mutation eliminated the tight Ca^{2+} regulation of vesicle fusion in PC12 cells. Disrupting the Ca^{2+} binding to the C2B in this background (Syt1$^{3A/F349A}$) had a small overall effect on vesicular exocytosis (Fig. 3*C*), with a near-identical number of exocytotic events observed under both basal and stimulating conditions compared with Syt1^{F349A} (Fig. 3*C*). Nonetheless, the number of constitutive exocytotic events was still significantly higher compared with the Syt1^{WT} rescue conditions (Fig. 3*C*). This implies that a significant portion of the exocytotic events observed with Syt1^{F349A} rescue are constitutive in nature (i.e., Ca^{2+}-independent), even under Ca^{2+}-stimulating conditions.

To verify that the phenotype observed under the Syt1^{F349A} rescue condition is specifically caused by disruption of the Syt1 oligomerization and to rule out any indirect or off-target effects, we tested and obtained similar results with two additional independent vesicle fusion reporters: Syt-pHluorin as a marker for small, clear vesicles and NPY-pHluorin as a dense-core vesicle marker (*SI Appendix*, Fig. S3). Additionally, we confirmed that expression levels of other PC12-associated Syt isoforms (Syt4, Syt7, and Syt9) and the SNARE proteins Syntaxin1 and SNAP25 (Fig. 3*A* and *SI Appendix*, Fig. S2) were unaltered by Syt1^{F349A} overexpression. Viewed together, these data strongly support the model that the C2B-dependent oligomerization of Syt1 suppresses spontaneous fusion events to enable Ca^{2+}-regulated vesicle exocytosis in PC12 cells. They further argue that the Ca^{2+}-dependent step of regulated exocytosis might primarily involve removing this inhibition on fusion machinery as opposed to direct activation of membrane fusion.

Discussion

The data presented here establish Syt1 oligomerization as a critical component of the Ca^{2+}-coupling mechanism. This follows from rescue experiments in Syt1-deficient PC12 cells (F7 cells) showing that disrupting the Syt1 oligomerization results in the abolition of Ca^{2+} control of exocytosis. In our pHluorin-based optical assay, we observe a significant reduction in overall exocytosis in the untransfected F7 cell line (Fig. 3*C*). However, earlier studies employing bulk secretion assays have reported little or no defect in Ca^{2+}-triggered exocytosis using the same cell line (27, 32). Under those conditions, increased expression of a closely related Syt isoform, Syt9, compensates for Syt1 deficiency, and, indeed, Syt1/Syt9 double deficiency results in complete loss of exocytosis (32, 33). In our untransfected F7 cell line, we observe a significant reduction (~50%) in the Syt9 expression levels in addition to Syt1 deficiency (Fig. 3*A*). Since the F7 cell line dates back ~25 y, genotypic and phenotypic variation could have occurred over an extended period of time (34–36). We believe that the combination of Syt1 deficiency and reduced Syt9 expression in our F7 cell line likely explains the strong loss-of-exocytosis phenotype observed (Fig. 3*C*). Consistent with the fusion phenotype, we also observe clear deficiency in docking of the dense-core vesicles in the untransfected F7 cells (Fig. 3*D*). It is worth noting that in our experimental conditions, overexpression of Syt1^{WT} was able to partially rescue the docking phenotype and fully restore the fusion properties, including the Ca^{2+}-regulated exocytosis, to the control PC12 cell levels (Fig. 3). This provides an ideal background to relate the effect of disrupting the oligomer formation using the Syt1^{F349A} mutant.

We further note that the observed effect of the Syt1 deficiency appears to be highly dependent on the choice of the reporter. Syt1 deficiency has been shown to increase the release of dopamine/ATP (27), to have no effect or drastically reduce the release of norepinephrine (32), to reduce the release of catecholamines, and to abolish NPY release (37, 38). In the current study, we use VAMP2-pHluorin, a universal reporter for exocytosis from all types of vesicles in PC12 cells. We additionally confirmed our fusion phenotype for untransfected and both WT and F349A rescue conditions using the independent reporters Syt-pHluorin and NPY-pHluorin, which are specific for small, clear vesicles and dense-core vesicles, respectively (*SI Appendix*, Fig. S3).

How does the Syt1 oligomerization reversibly clamp fusion? We envision a concerted mechanism wherein the full complement (15–20 copies) of Syt1 on the vesicle oligomerizes at the site of

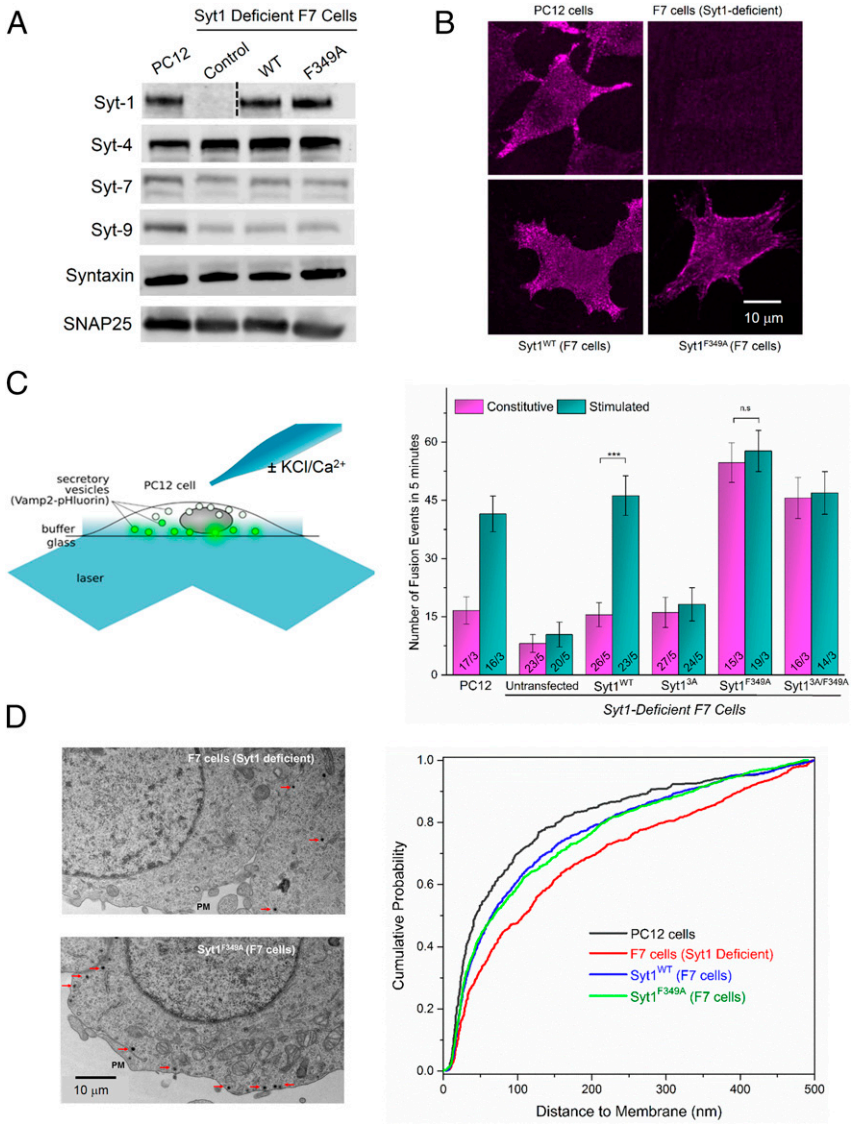

Fig. 3. Disrupting Syt1 oligomerization occludes Ca^{2+} control of exocytosis in PC12 cells. (*A*) Representative Western blot showing that untransfected F7 cells lack Syt1 expression along with reduced expression of Syt9, a closely related isoform. It further shows that the rescue of Syt1 expression in the F7 cells with $Syt1^{WT}$ or $Syt1^{F349A}$ leads to no alteration in the expression of other Syt isoforms and the SNARE proteins (quantitative analysis is provided in *SI Appendix*, Fig. S2). (*B*) Representative immunofluorescence analysis using anti-Syt1 antibody shows a similar distribution of the endogenous Syt1 in PC12 cells and the recombinant $Syt1^{WT}$ or $Syt1F^{349A}$ expressed in F7 cells. (*C*) Effect of $Syt1^{349A}$ mutation on exocytosis assessed by VAMP2-pHluorin TIRFM imaging of single-vesicle fusion events under basal (constitutive) conditions and after KCl-induced depolarization (stimulated with Ca^{2+}). Disrupting the Syt1 oligomer dysregulated exocytosis, dramatically increasing (approximately threefold) the typically low levels of constitutive exocytosis and effectively abolishing the Ca^{2+} control of exocytosis. The majority of the exocytotic events with $Syt1F^{349A}$ rescue are constitutive in nature, as disrupting Ca^{2+} binding ($Syt1^{3A/F349A}$) shows little or no effect under either basal or stimulated conditions. ***$P < 0.005$ Wilcoxon–Mann–Whitney test. n.s., not significant. (*D*) EM of serial sections was used to characterize the distribution and docking of the dense-core vesicles (DCVs). (*Left*) Representative micrograph of untransfected (*Top*) or $Syt1^{F349A}$-expressing (*Bottom*) F7 cells. The DCVs are marked by red arrows. (*Right*) Cumulative probability plots of DCV distribution relative to the PM. Untransfected F7 cells (red) showed a pronounced right shift in the distribution, with fewer vesicles locating near the PM ($P < 0.001$ vs. PC12 cells, Kolmogorov–Smirnov test). This impairment in vesicle docking is partially rescued by the expression of either $Syt1^{WT}$ or $Syt1^{F349A}$ (blue and green, respectively). Data are from $n = 14$–32 cells for each condition, with 55 ± 38 vesicles per cell (mean ± SD) from three independent preparations.

docking triggered by PIP2 binding (Fig. 4). It is then ideally positioned to simultaneously template multiple SNAREpins, likely using the recently identified "primary" binding site involving SNAP25 and the C2B domain (9, 18), which is accessible and free to interact in the ring oligomer (21). The height of Syt1 oligomers combined with the SNAREs atop would maintain the two bilayers far enough apart (~4 nm) to allow the N-terminal assembly but sterically block the complete assembly (18). The SNAREpin bound to the Syt1 ring oligomer would also be restrained from moving radially inward in the membrane plane, preventing full zippering (18). In this manner, the Syt1 oligomerization lowers the probability of the fusion of the docked vesicle in the absence of the Ca^{2+} trigger (Fig. 4).

It is possible that the C2B oligomers dynamically break and reform, and intact ring-like oligomers observed in vitro are not always present or predominant in vivo. Under these conditions, very short oligomers of Syt1 could serve to clamp SNAREpins by restraining them from rotating away from the ideal orientation in which C-terminal zippering is sterically prevented. However, such a stochastic mechanism would produce an inefficient clamp

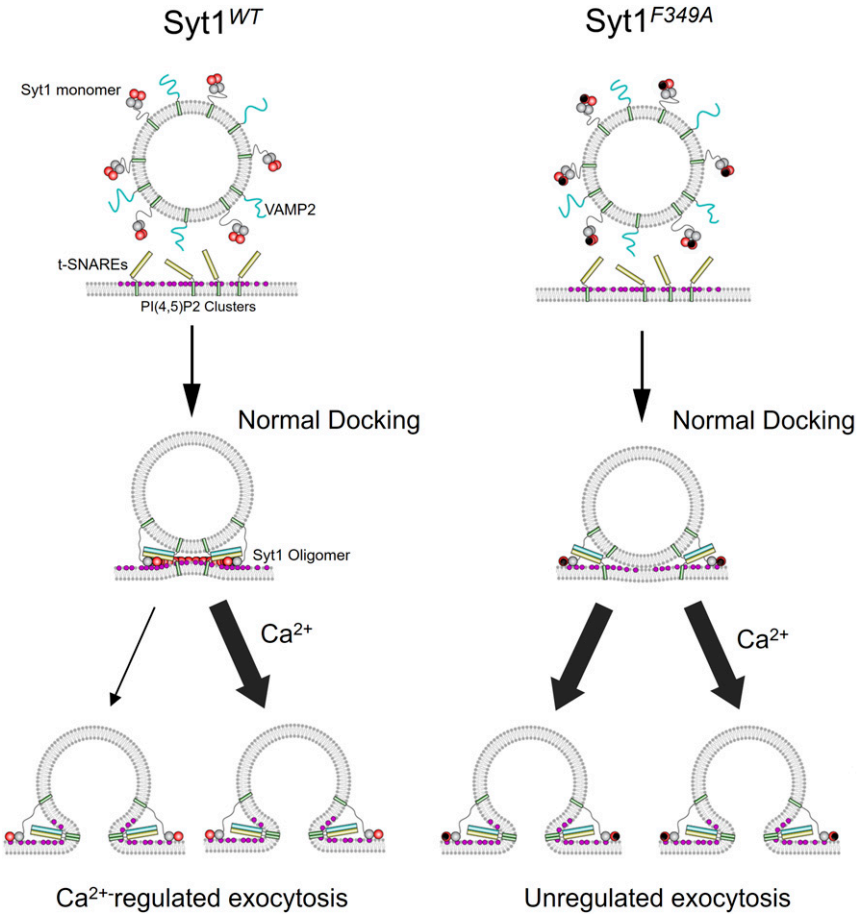

Fig. 4. Model for Ca^{2+}-regulated exocytosis. Oligomerization of the Syt1 regulates SNARE assembly at the site of docking; specifically, it prevents the terminal zippering by sterically blocking the close approach of the vesicle and by radially restricting the assembly process. This serves to reversibly clamp SNAREpins until they are dissociated by Ca^{2+} binding. In this manner, the Syt1 oligomerization imposes Ca^{2+} control on vesicle fusion. Disrupting the oligomerization (F349A mutation) does not affect the vesicle docking but removes the clamp to enhance the spontaneous fusion events, effectively abolishing Ca^{2+} control even though the Ca^{2+} activation mechanism is intact.

as the SNAREpin can "twist" out of position and complete zippering, leading to fusion (18). Thus, we favor a more concerted mechanism, in which in the Syt1 ring-like oligomers act as a "primer" to template and link multiple SNARE proteins and, along with the SNARE-associated chaperones (Munc13 and Munc18) and regulators (Complexin), enable rapid, Ca^{2+}-coupled vesicular release (18). Additionally, this arrangement would allow for binding of other Syt isoforms to the templated SNARE proteins via the conserved Complexin-dependent, "tripartite"-binding site (10), and thus provides a plausible framework to describe the synergistic action of different Syt isoforms (39). While the precise molecular architecture of the clamped state is still unclear, the Syt1 oligomer-based model provides the most elegant solution of a symmetrical structure that balances the physical forces to maximize stability before release (18).

The Syt1 oligomers are disassembled upon Ca^{2+} influx, which liberates the partially assembled SNAREpins to complete zippering and open the fusion pore cooperatively (Fig. 4). Syt1 oligomerization, by virtue of stabilizing the Ca^{2+}-binding loops at the dimer interface (20, 21), would also prevent any extemporary membrane insertion (40), and thus ensure vesicular release only when the critical intracellular [Ca^{2+}] is reached. Thus, the Syt1 oligomerization synchronizes vesicle fusion to Ca^{2+} influx. Additionally, our data suggest that the Ca^{2+}-triggered loop insertion of the Syt1 principally serves to reverse the "clamp" on the fusion machinery and that any additional contribution in promoting membrane fusion by lipid bilayer perturbations (41) plays an auxiliary role. This is an emerging and speculative concept (18, 42) and requires further research.

While the clustering of Syt at nerve terminals has been reported (43), the oligomeric structures (intact or dynamic) that we propose have not been directly observed. We note that the methods applied to date, both in vivo and in vitro, would not be expected to reveal these structures without intentional effort, particularly to preserve these metastable structures. Thereby, focused high-resolution structural studies within the cellular context will be needed to confirm the general outline of this model and to provide intimate details. Nevertheless, given that C2-domain oligomerization is a conserved feature among C2-domain proteins (21), many of which regulate exocytosis, we believe that diverse forms of intercellular communication and physiological response may also rely on similar clamping and triggering mechanisms to govern the fusion machinery.

Experimental Procedures

Materials. The following DNA constructs, which have been previously generated and sequenced (13, 19, 21, 44), were used: pCDFDuet-GST-PreScission-$Syt1^{C2AB}$ (rat Syt1 residues 143–421); pGEX GST-thrombin-$Syt1^{CD}$ (rat Syt1 residues 96–421) WT and single-cysteine mutants at residue 269 (E269C) and residue 304 (V304C); pET28a oligohistidine-thrombin-Syntaxin1A (rat Syntaxin1A residues 191–253), pET28a oligohistidine-SUMO-SNAP25A (residues 1–203); and pET15b-oligohistidine-thrombin-VAMP2 (human VAMP2 residues 1–96) with a single cysteine at residue 28 (S28C). In addition, the following

Syt1 mutants were created in this study: V304N, L307N, L307A, Y311N, F349N, F349A, and L394N in the $Syt1^{C2AB}$ background and F349A in the $Syt1^{CD}$ background using a QuikChange mutagenesis kit (Agilent Technologies). All recombinant proteins were expressed and purified as described previously (13, 19, 21, 44). The VAMP2-pHluorin construct used has been described previously (28). For the generation of the HA-tagged Syt1 plasmids used for transfections of F7 cells, the full-length rat Syt1 cDNA was cloned into a pCMV-HA-N vector (Clontech) that had been modified by inserting a 25-aa signal sequence of preprotachykinin upstream of the HA tag using the ApaI restriction site. The NPY-pHluorin construct was generated by amplifying human NPY from NPY-mCherry (catalog no. 67156; Addgene) and inserting it into the pCIneo vector (Promega) with a 6-aa linker upstream of a pHluorin tag. The pcDNA3 rat Syt-pHluorin construct was obtained from Addgene, Inc. (catalog no. 37003). The PC12 cell line was a gift from Barbara Ehrlich, Yale University, and the Syt1-deficient PC12 (termed F7) cells were purchased from RIKEN BRC (catalog no. RCB2800, RRID:CVCL_T752). The lipids 1-palmitoyl-2-oleoyl-sn-glycero-3-phosphocholine, 1,2-dioleoyl-sn-glycero-3-phospho-L-serine, and PIP2 were purchased from Avanti Polar Lipids. The thiol-reactive fluorescent probes Alexa Fluor 488-maleimide and IANBD Amide [*N*,*N*′-dimethyl-*N*-(iodoacetyl)-*N*′-(7-nitrobenz-2-oxa-1,3-diazol-4-yl)ethylenediamine] were purchased from Thermo Scientific.

Lipid Monolayer Assay. The monolayers were set up as described previously (19, 21). Briefly, degassed ultrapure H_2O was injected through a side port to fill up wells (4-mm diameter, 5-mm depth) in a Teflon block. The flat-water surface was coated with 0.6 μL of phospholipid mixture. The following lipid mixtures were used: PC/PS with molar ratio of 60:40 (for $Syt1^{C2AB}$ experiments) or PC/PS/PIP2 with molar ratio of 72.5:25:2.5 (for $Syt1^{CD}$ experiments), which were premixed as required, dried under N_2 gas, and then resuspended in chloroform to a final total lipid concentration of 0.5 mM. The Teflon block then was stored in a sealed humidity chamber for 1 h at room temperature to allow the chloroform to evaporate. Continuous carbon-coated EM grids were baked at 70 °C for 4 h and washed with hexane to improve hydrophobicity. Lipid monolayers formed at the air/water interface were then recovered by placing the pretreated EM grid (400 mesh; Ted Pella) carbon side down on top of each water droplet for 1 min. The grid was raised above the surface of the Teflon block by injecting ultrapure H_2O into the side port and then was lifted off the droplet immediately.

Proteins were rapidly diluted to 3 μM in 20 mM 3-(*N*-morpholino)propanesulfonic acid (pH 7.5), 15 mM KCl, 1 mM EDTA, 2 mM $MgAC_2$, 1 mM DTT, and 5% (wt/vol) trehalose buffer, and were then added to the lipid monolayer on the grid and incubated in a 37 °C humidity chamber for 1 min. The final KCl concentration in the buffer was adjusted to 100 mM as required. To facilitate structural analysis of the ring-like structures, we further optimized the incubation conditions by using an annealing procedure: Rings were nucleated at 37 °C for 1 min, followed by a 30-min annealing step at 4 °C. The grids were rinsed briefly (~10 s) with incubation buffer alone or with buffer supplemented with $CaCl_2$ (0.1, 0.5, and 1 mM free) for Ca^{2+} treatment studies. The free [Ca^{2+}] was calculated by Maxchelator (maxchelator.stanford.edu). Subsequently, the grids were blotted with Whatman no.1 filter paper, negatively stained with uranyl acetate solution (1% wt/vol), and air dried. The negatively stained specimens were examined on an FEI Tecnai T12 microscope operated at 120 kV. The defocus range used for our data was 0.6–2.0 μm. Images were recorded under low-dose conditions (~20 $e^-/Å^2$) on a 4K × 4K CCD camera (UltraScan 4000; Gatan, Inc.) at a nominal magnification of 42,000×. Micrographs were binned by a factor of 2 at a final sampling of 5.6 Å per pixel on the object scale. The image analysis, including size distribution measurements, was carried out using ImageJ software (NIH).

Liposome Flotation Assay. Ca^{2+}-independent Syt1-membrane interaction was measured using a liposome floatation assay as described previously (21). $Syt1^{CD}$ (WT and F349A) was incubated with PS/PIP2 liposomes (71.5% PC, 25% PS, 2.5% PIP2, 1% NBD) for 1 h at room temperature and separated using a discontinuous Nycodenz (Sigma–Aldrich) gradient. The bound fraction (normalized to the lipid using NBD fluorescence) was then estimated by densitometry analysis of SDS/PAGE gels using ImageJ software (45).

MST Analysis. $Syt1^{WT}$, $Syt1^{F349A}$, and $Syt1^{L307A}$ interaction with Ca^{2+} and the SNARE complex was quantified using MST (NanoTemper Technologies GmbH) as described previously (46). For Ca^{2+}-binding analysis, MST was measured with ~50 nM $Syt1^{CD}$ (WT, L307A, and F349A) labeled with Alexa Fluor 488 at residue 269 (E269C) in 25 mM Hepes, 100 mM KCl, 2.5 mg/mL BSA, and 0.5% Tween (pH 7.4) using premium coated capillaries. Similar conditions and setup were used to measure Syt1–SNARE interaction, but using ~10 nM Alexa Fluor 488-labeled preassembled SNARE complex (VAMP2 residue 28) and unlabeled Syt1 (WT and F349A). The MST curves were fitted with simple Michaelis–Menten kinetics to obtain the apparent dissociation constant for Ca^{2+} and SNARE binding. (Note: For the Syt1–SNARE interaction studies, MST data beyond 50 μM Syt1 concentration were not included in the analysis due to precipitation of Syt1 protein at high concentrations under these experimental conditions.)

Stopped-Flow Rapid Mixing Analysis. To monitor Ca^{2+}-triggered membrane interaction of the Syt1 (WT and F349A), the tips of the Ca^2-binding loops of the C2B domain ($Syt1^{CD}$ residue 304) were labeled with an environment-sensitive probe, NBD. Stopped-flow rapid mixing analysis was carried out using an Applied Photophysics SX20 instrument, as described previously (13), with the fluorescently labeled Syt1 preincubated with PS/PIP2 liposome (72% PC, 25% PS, 3% PIP2) loaded in one syringe and buffer containing EGTA or Ca^{2+} in the other syringe. The samples were mixed rapidly (dead time ~ 1 ms), yielding a final concentration of 0.2 mM EGTA and 1 mM Ca^{2+}. The change in fluorescence signal collected with a 510-nm cutoff filter (Excitation 460 nm) was fitted with a single exponential function to calculate the observed rate of insertion of the Ca^{2+} loops.

Live Cell Imaging. PC12 cells and the Syt1-deficient F7 cells (27) were incubated at 37 °C in 5% CO_2 in DMEM, supplemented with 10% horse serum, 5% FBS, MEM nonessential amino acid solution, 1 mM sodium pyruvate, and 100 μg/mL penicillin/streptomycin (Gibco). F7 cells were cultured in tissue culture flasks pretreated with fibronectin or collagen-4 as they were not as adherent as the WT PC12 cells. F7 cells were electroporated using the Amaxa Nucleofector method (VVCA-1003KT; Lonza) with ~1–1.5 μg of Vamp2-pHluorin plasmid DNA and ~1–1.5 μg of either $Syt1^{WT}$ or $Syt1^{F349A}$ plasmid DNA, with a typical transfection efficiency of ~60%. Protein expression was verified by Western blot analysis using a mouse anti-Syt1 antibody (Synaptic Systems). For imaging, cells were plated on 35-mm tissue culture dishes with a cover glass bottom (refractive index = 1.51; World Precision Instruments), precoated with poly-D-lysine and fibronectin, and imaged 48 h later. Medium was replaced with Live Cell Imaging Solution (Thermo Fisher Scientific) supplemented with 1.3 mM Ca^{2+}, and cells were imaged at 37 °C using a custom-made TIRFM (30, 31, 47, 48) setup based on an Olympus IX-70 inverted microscope fitted with a 1.45-N.A./60× TIRFM lens (Olympus) and controlled by μManager software (www.micro-manager.org). The pHluorin was excited by the 488-nm line of an Innova 70C-Spectrum ion laser (Coherent). Cells were imaged at 6.6 Hz with 150-ms exposure using a Zyla 4.2 Megapixel Camera (Andor Technologies). The emission was collected through a BrightLine full-multiband laser filter set, optimized for 405-, 488-, 561-, and 635-nm laser sources (part no. LF405/488/561/635-A-000; Semrock). PC12 cells were stimulated for exocytosis in Live Cell Imaging Solution (Thermo Fisher Scientific). The tip of a micropipette containing a stimulating solution (Live Cell Imaging Solution with 1.3 mM $CaCl_2$ and 100 mM KCl) was positioned near the target cell with a micromanipulator (Warner Instruments). The stimulating solution was pressure ejected with Picospritzer II (Parker Instrumentation, General Valve Division). Single-vesicle exocytosis events were automatically detected using MATLAB (MathWorks) software as described previously (30, 31, 47, 48). The statistical significance of the fusion results was established using a Wilcoxon–Mann–Whitney test to account for the nonnormal distribution of the data using the open-source software Gnumeric (www.gnumeric.org).

Immunoblot Analysis. Cells (cultured PC12, Syt1-deficient F7 cells and F7 cells transfected with either $Syt1^{WT}$ or $Syt1^{F349A}$) were grown in six-well plates. After 48 h, cells were washed, detached, and collected by centrifugation. Pellets were resuspended in radioimmunoprecipitation assay buffer for 3–5 h, followed by spin down at top speed (20,817 × *g*) in a bench-top centrifuge for 30 min. Protein estimation in the postnuclear cell lysates was performed using bicinchoninic acid assay reagent from Pierce. An equal quantity (~15–20 μg) of protein from four cell lysates was first separated in SDS/PAGE and then transferred onto PVDF membranes (Millipore) for immune blotting. After being blocked with Odyssey Blocking Buffer (LI-COR Biosciences), the membranes were incubated with appropriate primary antibodies. The following primary antibodies from Synaptic Systems were used: Syt1 (catalog no. 105011), Syt9 (catalog no. 105053), Syt4 (catalog no. 105043), Syt7 (catalog no. 105173), SNAP25 (catalog no. 111011), and Syntaxin1 (catalog no. 110011). The levels of individual proteins were determined by quantitative Western blots with IRDye-conjugated secondary antibodies (IRDye 680RD goat anti-mouse IgG or IRDye 680RD goat anti-rabbit IgG) on a LI-COR infrared imaging system. Fluorographs were quantitatively scanned using ImageStudio.

Immunofluorescence. Cells (cultured PC12, Syt-1–deficient F7 cells and F7 cells transfected with $Syt1^{WT}$ or $Syt1^{F349A}$) on coverslips, pretreated with poly-D-lysine and fibronectin, were fixed and prepared for immunofluorescence against Syt1 [mouse Syt1 antibody tagged with Oyster 550 (Synaptic Systems)].

EM Analysis. Cultured PC12, Syt-1 deficient F7 cells, and F7 cells transfected with either Syt1-WT or Syt1-F349A on coverslips, pretreated with poly-D-lysine and fibronectin, were fixed in 2.5% glutaraldehyde in 0.1 M sodium cacodylate buffer (pH 7.4) at room temperature for 1 h. The cells were then rinsed twice in the same buffer and postfixed in 0.5% osmium tetroxide (OsO_4) at room temperature for 30 min, followed by another 30 min in 1% tannic acid solution. Specimens were stained *en bloc* with 2% aqueous uranyl acetate for 15 min, dehydrated in a graded series of ethanol to 100%, and embedded in Poly/Bed 812 resin. Blocks were polymerized in a 60 °C oven for 24 h. Thin sections (60 nm) were cut using a Leica ultramicrotome and poststained with 2% uranyl acetate and lead citrate. Cell sections were examined with an FEI Tecnai transmission electron microscope at an accelerating voltage of 80 kV; digital images were recorded with an Olympus Morada CCD camera and iTEM imaging software. ImageJ software (45) was used to measure the distance of each individual dense-core vesicle from the closest PM (outer membrane – outer membrane distance). An average of 10–15 cells per condition with a minimum of ~500 vesicles was used to create the cumulative distribution plot.

ACKNOWLEDGMENTS. We thank the NIH (Grant DK027044 to J.E.R.) for support of this research. This work was also supported by the Wellcome Trust Strategic Award (Reference 104033) (to J.E.R. and K.E.V.). We thank Dr. Xinran Liu and Morven Graham at the Center for Cellular and Molecular Imaging EM Core Facility, Yale School of Medicine, for technical input and support.

1. Burgess TL, Kelly RB (1987) Constitutive and regulated secretion of proteins. *Annu Rev Cell Biol* 3:243–293.
2. Gerber SH, Südhof TC (2002) Molecular determinants of regulated exocytosis. *Diabetes* 51(Suppl 1):S3–S11.
3. Südhof TC (2013) Neurotransmitter release: The last millisecond in the life of a synaptic vesicle. *Neuron* 80:675–690.
4. Söllner T, et al. (1993) SNAP receptors implicated in vesicle targeting and fusion. *Nature* 362:318–324.
5. Weber T, et al. (1998) SNAREpins: Minimal machinery for membrane fusion. *Cell* 92: 759–772.
6. Brose N, Petrenko AG, Südhof TC, Jahn R (1992) Synaptotagmin: A calcium sensor on the synaptic vesicle surface. *Science* 256:1021–1025.
7. Fernández-Chacón R, et al. (2001) Synaptotagmin I functions as a calcium regulator of release probability. *Nature* 410:41–49.
8. Geppert M, et al. (1994) Synaptotagmin I: A major Ca2+ sensor for transmitter release at a central synapse. *Cell* 79:717–727.
9. Zhou Q, et al. (2015) Architecture of the synaptotagmin-SNARE machinery for neuronal exocytosis. *Nature* 525:62–67.
10. Zhou Q, et al. (2017) The primed SNARE-complexin-synaptotagmin complex for neuronal exocytosis. *Nature* 548:420–425.
11. Rhee JS, et al. (2005) Augmenting neurotransmitter release by enhancing the apparent Ca2+ affinity of synaptotagmin 1. *Proc Natl Acad Sci USA* 102:18664–18669.
12. Paddock BE, et al. (2011) Membrane penetration by synaptotagmin is required for coupling calcium binding to vesicle fusion in vivo. *J Neurosci* 31:2248–2257.
13. Krishnakumar SS, et al. (2013) Conformational dynamics of calcium-triggered activation of fusion by synaptotagmin. *Biophys J* 105:2507–2516.
14. Bai J, Tucker WC, Chapman ER (2004) PIP2 increases the speed of response of synaptotagmin and steers its membrane-penetration activity toward the plasma membrane. *Nat Struct Mol Biol* 11:36–44.
15. Bai J, Wang P, Chapman ER (2002) C2A activates a cryptic Ca(2+)-triggered membrane penetration activity within the C2B domain of synaptotagmin I. *Proc Natl Acad Sci USA* 99:1665–1670.
16. Paddock BE, Striegel AR, Hui E, Chapman ER, Reist NE (2008) Ca2+-dependent, phospholipid-binding residues of synaptotagmin are critical for excitation-secretion coupling in vivo. *J Neurosci* 28:7458–7466.
17. Bacaj T, et al. (2013) Synaptotagmin-1 and synaptotagmin-7 trigger synchronous and asynchronous phases of neurotransmitter release. *Neuron* 80:947–959.
18. Rothman JE, Krishnakumar SS, Grushin K, Pincet F (2017) Hypothesis - Buttressed rings assemble, clamp, and release SNAREpins for synaptic transmission. *FEBS Lett* 591: 3459–3480.
19. Wang J, et al. (2014) Calcium sensitive ring-like oligomers formed by synaptotagmin. *Proc Natl Acad Sci USA* 111:13966–13971.
20. Wang J, et al. (2017) Circular oligomerization is an intrinsic property of synaptotagmin. *eLife* 6:e27441.
21. Zanetti MN, et al. (2016) Ring-like oligomers of synaptotagmins and related C2 domain proteins. *eLife* 5:e17262.
22. Parisotto D, Malsam J, Scheutzow A, Krause JM, Söllner TH (2012) SNAREpin assembly by Munc18-1 requires previous vesicle docking by synaptotagmin 1. *J Biol Chem* 287: 31041–31049.
23. Loewen CA, Lee SM, Shin YK, Reist NE (2006) C2B polylysine motif of synaptotagmin facilitates a Ca2+-independent stage of synaptic vesicle priming in vivo. *Mol Biol Cell* 17:5211–5226.
24. Honigmann A, et al. (2013) Phosphatidylinositol 4,5-bisphosphate clusters act as molecular beacons for vesicle recruitment. *Nat Struct Mol Biol* 20:679–686.
25. Burgoyne RD, Morgan A (1998) Analysis of regulated exocytosis in adrenal chromaffin cells: Insights into NSF/SNAP/SNARE function. *BioEssays* 20:328–335.
26. Westerink RH, Ewing AG (2008) The PC12 cell as model for neurosecretion. *Acta Physiol (Oxf)* 192:273–285.
27. Shoji-Kasai Y, et al. (1992) Neurotransmitter release from synaptotagmin-deficient clonal variants of PC12 cells. *Science* 256:1821–1823.
28. Miesenböck G, De Angelis DA, Rothman JE (1998) Visualizing secretion and synaptic transmission with pH-sensitive green fluorescent proteins. *Nature* 394:192–195.
29. Coleman J, et al. (2018) PRRT2 regulates synaptic fusion by directly modulating SNARE complex assembly. *Cell Rep* 22:820–831.
30. Sebastian R, et al. (2006) Spatio-temporal analysis of constitutive exocytosis in epithelial cells. *IEEE/ACM Trans Comput Biol Bioinformatics* 3:17–32.
31. Toomre D (2012) Generating live cell data using total internal reflection fluorescence microscopy. *Cold Spring Harb Protoc* 2012:439–446.
32. Fukuda M, Kowalchyk JA, Zhang X, Martin TF, Mikoshiba K (2002) Synaptotagmin IX regulates Ca2+-dependent secretion in PC12 cells. *J Biol Chem* 277:4601–4604.
33. Lynch KL, Martin TF (2007) Synaptotagmins I and IX function redundantly in regulated exocytosis but not endocytosis in PC12 cells. *J Cell Sci* 120:617–627.
34. Geraghty RJ, et al.; Cancer Research UK (2014) Guidelines for the use of cell lines in biomedical research. *Br J Cancer* 111:1021–1046.
35. Lorsch JR, Collins FS, Lippincott-Schwartz J (2014) Cell biology. Fixing problems with cell lines. *Science* 346:1452–1453.
36. Sato S, Rancourt A, Sato Y, Satoh MS (2016) Single-cell lineage tracking analysis reveals that an established cell line comprises putative cancer stem cells and their heterogeneous progeny. *Sci Rep* 6:23328.
37. Moore JM, Papke JB, Cahill AL, Harkins AB (2006) Stable gene silencing of synaptotagmin I in rat PC12 cells inhibits Ca2+-evoked release of catecholamine. *Am J Physiol Cell Physiol* 291:C270–C281.
38. Roden WH, et al. (2007) Stable RNA interference of synaptotagmin I in PC12 cells results in differential regulation of transmitter release. *Am J Physiol Cell Physiol* 293: C1742–C1752.
39. Volynski KE, Krishnakumar SS (2018) Synergistic control of neurotransmitter release by different members of the synaptotagmin family. *Curr Opin Neurobiol* 51:154–162.
40. Gruget C, et al. (2018) Rearrangements under confinement lead to increased binding energy of synaptotagmin-1 with anionic membranes in Mg^{2+} and Ca^{2}. *FEBS Lett* 592: 1497–1506.
41. Martens S, Kozlov MM, McMahon HT (2007) How synaptotagmin promotes membrane fusion. *Science* 316:1205–1208.
42. Brunger AT, Leitz J, Zhou Q, Choi UB, Lai Y (April 26, 2018) Ca^{2+}-triggered synaptic vesicle fusion initiated by release of inhibition. *Trends Cell Biol*, 10.1016/j.tcb.2018.03.004.
43. Willig KI, Rizzoli SO, Westphal V, Jahn R, Hell SW (2006) STED microscopy reveals that synaptotagmin remains clustered after synaptic vesicle exocytosis. *Nature* 440: 935–939.
44. Krishnakumar SS, et al. (2011) A conformational switch in complexin is required for synaptotagmin to trigger synaptic fusion. *Nat Struct Mol Biol* 18:934–940.
45. Schneider CA, Rasband WS, Eliceiri KW (2012) NIH Image to ImageJ: 25 years of image analysis. *Nat Methods* 9:671–675.
46. van den Bogaart G, Meyenberg K, Diederichsen U, Jahn R (2012) Phosphatidylinositol 4,5-bisphosphate increases Ca2+ affinity of synaptotagmin-1 by 40-fold. *J Biol Chem* 287:16447–16453.
47. Xu Y, et al. (2011) Dual-mode of insulin action controls GLUT4 vesicle exocytosis. *J Cell Biol* 193:643–653.
48. Rivera-Molina F, Toomre D (2013) Live-cell imaging of exocyst links its spatiotemporal dynamics to various stages of vesicle fusion. *J Cell Biol* 201:673–680.